J. Fluid Mech. (2008), *vol.* 606, *pp.* 399–415.
doi:10.1017/S0022112008001985 Printed in the United Kingdom

Direct numerical simulation of three-dimensional turbulent rough channels: parameterization and flow physics

P. ORLANDI[1] AND S. LEONARDI[2]

[1]Dipartimento di Meccanica e Aeronautica Università La Sapienza, Via Eudossiana 18, 00184, Roma, Italy

[2]Department of Mechanical Engineering, University of Puerto Rico at Mayaguez, Mayaguez 00680-9045 Puerto Rico

(Received 23 October 2007 and in revised form 7 April 2008)

Direct numerical simulations of the three-dimensional flow past rough surfaces with elements of different shapes are performed to create a database. Our main interest is in finding a new parameterization for turbulent rough flows, which, so far, has been based on the concept of equivalent sand grain height or on the net separation between k and d type roughnesses. The new parameterization permits us to find a simple expression for the roughness function and the root mean square of the normal velocity fluctuation at the plane of the crests. We also wish to find statistical quantities characterizing the effects of the different rough surfaces: one is the ratio between mean flow and turbulence time scales (Sq/ϵ), the other is the helicity density. Passive scalar visualizations evince a reduction of the wall streak coherence, and the absence of a signature of the rough surfaces on the passive scalar distribution. The tendency towards a flow isotropy near the roughness has been explained also through Sq/ϵ.

1. Introduction

Nikuradse (1933) in his landmark paper on turbulent rough walls, presented a large number of measurements in pipes with walls covered by sand grain; he described in detail, the efforts made to prepare the rough surfaces. The pattern of the surfaces had a random character (Nikuradse 1933, p. 49 microphotograph), which is common in several rough walls, for instance in ship hulls, or, at greater scales, on terrains such as canopies or different kinds of vegetation. Nikuradse (1933) showed that by plotting the friction factor versus the Reynolds number, three regimes are encountered: in the first one, at low Re, the friction follows the law of laminar smooth walls, and does not depend on the roughness. In the transitional regime, the friction depends on Re and on the kind of roughness. At higher Re there is a regime where the friction depends on the kind of roughness, and not on Re. In these conditions the flow was defined as fully rough. This result can be of significant interest to those performing DNS (direct numerical simulations), suggesting that the near-wall physics can be studied at low Reynolds numbers. On the other hand, for smooth walls, expensive simulations, such as those by del Álamo *et al.* (2004), permitted us to understand fully the physics of wall turbulent flows, and its dependence on the Reynolds number. The reason for the different behaviour between smooth and rough flows, relies on the nature of friction; in the former, only viscous drag is present, whereas in the latter, the form

drag prevails over the viscous drag. For rough flows, the ratio between form and friction drag depends on the shape of the surface. In laboratory experiments, it is difficult to separate the two effects, but in numerical experiments this can be done, (Leonardi *et al.* 2003; Orlandi, Leonardi & Antonia 2006).

The weak point of Nikuradse's (1933) experiments is the lack of reproducibility of the rough surfaces. Schlichting (1936) criticized the lack of reproducibility: 'One objection to using sand roughness, as a standard, is that this type is not satisfactorily reproducible. If, for example, instead of employing lacquer for gluing the sand to the plates, as was done by Nikuradse, we used some other binding material, and if the time taken for drying was chosen somewhat differently, another sand-grain density and therefore a different resistance, would result.' Schlichting (1936) inserted, in the same apparatus as used by Nikuradse, three-dimensional roughness surfaces of different shapes, for instance spheres, spherical segments, cones, long and short angle prisms. The large impact of the Nikuradse study, influenced Schlichting to evaluate the equivalent sand grain roughness height K_S, and to express the velocity profiles in wall units as

$$U^+ = 8.48 + 5.75\log((y+\delta)/K_S), \quad 5.75 = \log_{10}/\kappa, \tag{1.1}$$

giving a very good fit of the data. The velocity U was scaled with the rough friction velocity $u_{\tau R}$, obtained by the resistance factor $\lambda = (\mathrm{d}p/\mathrm{d}x)4r_h/\rho U_b^2$, with r_h the hydraulic radius, κ the Kármán constant, U_b the bulk velocity and $(\mathrm{d}p/\mathrm{d}x)$ was measured by pressure taps on the walls. The effective origin δ, and K_S were determined by a best fit of the data in the log region. The detailed evaluation of K_S is described by Nikuradse (1933 pp. 15, 16).

Considering the time when these experiments were performed, the results had a significant impact. The equivalent height K_S is a quantity without an exact physical meaning, but useful and necessary for a good fit of the experimental data. On similar grounds, several years later, for rough surfaces of simple shape, such as square or two-dimensional rods, a classification of rough surfaces as k and d type was introduced by Perry, Schofield & Joubert (1969). In addition, attempts were made to express the roughness function through a combination of geometrical parameters. Waigh & Kind (1998) collected, from the literature, measurements of 64 rough surface experiments, covering a wide range of roughness element shapes (cubes, cylinders, cones, spheres and hemispheres). They found two classes of roughness, but arbitrariness in the procedure, and a lack of physics were present. We believe that it is important, as suggested by Belcher, Jerram & Hunt (2003), to find a better parameterization for rough surfaces, in particular for dealing with real rough flows, such as those in turbine blades, or in micrometereological applications. In predicting real flows, turbulence models are required, therefore, a better parameterization could be achieved through the variables in the turbulence models, for instance the Reynolds stresses. These statistics, at the surface of the roughness, or better near the interface between the roughness and the flow, depend on the shape of the surface. In a laboratory, it is difficult to measure the three velocity components, because the hot wire or the laser beam cannot be located at the plane of the roughness crest. The measurement of the other quantities, for instance the vorticity components and the pressure in the inner region, are even more difficult. Understanding of all the details of the near-wall physics relies on the DNS at low Reynolds number, but the DNS must be validated.

Orlandi *et al.* (2006) validated the numerical simulations by a comparison of the pressure distribution on two-dimensional rods, with that measured by Furuya, Miyata & Fujita (1976). Regarding the flow physics, Leonardi *et al.* (2003) explained

why maximum drag is achieved for square bars at $w/k = 7$ (w is the separation between the square bars, and k is the height of the elements). Moreover, Orlandi *et al.* (2003) demonstrated that the normal velocity distribution on the plane of the crests is the driving mechanism for the modifications of the near-wall structures. The preliminary results suggested that, a new parameterization for rough flows could be obtained by $\tilde{u}_2'|_w$, with $\tilde{u}_i' = \langle u_i'^2 \rangle^{1/2}$. (angle brackets $\langle\rangle$ indicate averages in the homogeneous directions and in time, and $|_w$ values at the plane of the crests). A continuous transition between smooth ($\tilde{u}_2'|_w = 0$) and rough walls ($\tilde{u}_2'|_w \neq 0$) is then reached, avoiding the sharp transition between k and d type rough surfaces. A useful parameterization should lead to an expression for U^+, similar to (1.1), but K_S should be substituted by a quantity with a physical meaning, for example, a quantity controlling the near-wall vortical structures. To have wide validity, the law should be verified for a large number of different rough surfaces; Orlandi & Leonardi (2006) for two- and three-dimensional roughness found a very good correlation between the roughness function ΔU^+ and $\tilde{u}_2'|_w$.

The roughness function introduced by Hama (1954), is based on the assumption that for flows past rough surfaces the log-law (Clauser 1954) is also valid, but it is shifted downward by ΔU_C^+. The expression is

$$U^+ = \kappa^{-1} \ln(y^+) + B - \Delta U_C^+. \tag{1.2}$$

The distance in wall units (y^+) is scaled with $\nu/u_{\tau R}$. B is a constant approximately equal to 5.5 for channel flows, and ΔU_C^+ is the roughness function proportional to k^+, which depends on the density and shape of the roughness elements and on the Reynolds number. The effective origin of y is at a distance d_0 from the roughness crest plane, which can be defined in several ways, as was discussed by Leonardi *et al.* (2003). Perry *et al.* (1969), Raupach, Antonia & Rajagopalan (1991) and Jiménez (2004) using Hama's (1954) expression found that, for k type roughness, there is a correlation between ΔU_C^+ and k^+:

$$\Delta U_C^+ = \kappa^{-1} \ln\, k^+ + C\ . \tag{1.3}$$

C depends on the roughness density and on the shape of the elements. Orlandi *et al.* (2006) by DNS of turbulent channel flow with square, circular and triangular rods, used a slightly different expression for the mean velocity profile in wall units. Instead of having an error in origin, d_0, dependent on the shape of the roughness, they imposed $d_0 = 0$. Therefore, the effective origin of y coincides with the plane of the crests. At this location, depending on the shape of the surface, there is a mean velocity $U_0 = \langle u_1 \rangle (y = 0) \neq 0$. For surfaces with elements of the same height, $y = 0$ is a simple assumption. For surfaces with elements of different heights (not considered in this paper), the best choice is to take the plane, passing through the highest points. On this plane, the averaged quantities U_0, $\tilde{u}_2'|_w$ and $\langle u_2' u_1' \rangle|_w$ can be obtained. With this choice, everything discussed here is still valid. Relative to this origin, the mean velocity in wall units is $\tilde{U}^+ = (\langle u_1 \rangle - U_0)/u_{\tau R}$. In the log-region, (1.2) becomes

$$\tilde{U}^+ = \kappa^{-1} \ln(\tilde{y}^+) + B - \Delta U^+, \tag{1.4}$$

where ΔU^+ is different from ΔU_C^+.

The aim of the present paper and of Orlandi *et al.* (2006) and Orlandi & Leonardi (2006) is to investigate the possibility of producing a universal parameterization of ΔU^+ with $\tilde{u}_2'|_w$. DNSs of flows past three-dimensional surfaces with a well-defined shape are performed following Schlichting's (1936) decision to insert regular three-dimensional elements in the channel. Here, the DNSs of random surfaces

are discarded because they require an enormous computational effort, and three-dimensional ordered structures are sufficiently complex to generate intense normal velocity fluctuations at the plane of the crests.

Efficient numerical tools allow us to perform DNS of flows past complex rough surfaces, for instance, Bhaganagar, Kim & Coleman (2004) considered an egg carton surface, where weak changes on the near-wall structures were observed, and these remain coherent in the streamwise direction. Coceal *et al.* (2006) considered staggered cubes; by free-slip conditions on the upper surface, they intended to reproduce flows similar to those over urban roughness. In the present paper, DNSs are performed to create a database with different kinds of roughness shapes, and in particular those producing large $\tilde{u}_2'|_w$. Wedges with different orientation, cylindrical protuberances, square cubes and combinations of those have been considered, which together with the previous data allow us to derive a useful expression for the parameterization of the roughness function. This could be of help in theoretical considerations or in numerical simulations with engineering turbulence closures to obtain results for real applications.

An accurate and fast numerical method is necessary to perform simulations where the shape of the geometry plays an important role. Orlandi & Leonardi (2006) explained why a second-order accurate staggered finite-difference scheme (Orlandi 2000) together with an efficient immersed boundary technique (Leonardi & Orlandi 2004) was used. A brief description of the numerical method is given in the following section.

2. Numerical procedure

The non-dimensional Navier–Stokes and continuity equations for incompressible flows are:

$$\frac{\partial u_i}{\partial t} + \frac{\partial u_i u_j}{\partial x_j} = -\frac{\partial p}{\partial x_i} + \frac{1}{Re}\frac{\partial^2 u_i}{\partial x_j^2} + \Pi\delta_{i1}, \qquad \frac{\partial u_j}{\partial x_j} = 0, \tag{2.1}$$

where Π is the pressure gradient required to maintain a constant flow rate, u_i is the component of the velocity vector in the i direction and p is the pressure. The reference velocity is the centreline laminar velocity profile U_P, the reference length is the half-channel width h, hence in (2.1), t is a dimensionless time, and x_i are dimensionless coordinates. The Navier–Stokes equations have been discretized in an orthogonal coordinate system through a staggered central second-order finite-difference approximation. The discretization scheme of the equations is reported in Orlandi (2000, chap. 9). To treat complex boundaries, in Fadlun *et al.* (2000), the velocities were set equal to zero in the solid, and, at the points closest to the boundary, were evaluated by linear interpolations. This assumption, for several flows is satisfactory because, near a solid boundary, the flow physics implies an almost linear velocity profile. An attempt was made to apply the linear interpolation to a turbulent channel with smooth walls, and a constant flow rate was not maintained. Leonardi & Orlandi (2004) modified the immersed boundary technique, for constant-flow-rate turbulent-channel simulations with surfaces of any shape.

In comparison with smooth channels, at the same Re, a larger number of points is necessary to describe the contour of the rough surface. To maintain a constant flow rate, Π in (2.1), has to balance the friction and pressure drag. Π is evaluated during the calculation of the right-hand side of (2.1). In a smooth channel, the staggered conservative scheme furnishes Π by the appropriate volume normalization

of the sum of the right-hand side of (2.1). In the presence of rough walls, after the discrete integration of the right-hand side of (2.1) in the whole computational domain, to account for the metric variations near the body, a correction is necessary. This procedure requires a number of operations proportional to the number of boundary points, and the flow rate remains constant within round-off errors. In principle, there are not large differences in treating two- or three-dimensional geometries. However, in the latter case, a greater memory store is necessary to define the nearest points to the surface.

A possible criticism of the capability of the method to deal with complex geometries is that, in contrast to methods based on a body-fitted coordinate system (Orlandi 1989), an infinitely small resolution is required. As the latter requirement is beyond our reach, the discrete representation of the roughness elements introduces small-scale disturbances related to the grid size, since these disturbances are generated at a rather small local Reynolds number, they are rapidly dissipated and therefore are not important. The corroboration of the previous discussion was presented in Orlandi *et al.* (2006) by a comparison of the pressure distribution on the rod elements with that measured by Furuya *et al.* (1976). They studied the boundary layer over two-dimensional circular rods, fixed to the wall transversely to the flow, for several values of w/k. The results presented for numerical validation, accounted for values of $w/k = 3, 7$ and 15; in addition, it is important to point out that circular rods are appropriate for numerical validation, because of the variation of the metric along the circle. The pressure accounts for the form drag which, for these values of w/k, overcomes the frictional drag. The numerical simulations for circular rods were performed, at $Re = U_P h/\nu = 4200$, in a channel with one wall smooth and the other rough. The good agreement implies that the numerical method is accurate and can be used to reproduce the flow past any kind of surface. The agreement between low-Re simulations and high-Re experiments (Furuya *et al.* 1976) implies a similarity, in the near-wall region, between boundary layers and channel flows. In addition, it can be asserted that, as in fully rough flows (Nikuradse 1933), a Reynolds-number independence does exist. To our knowledge, this detailed comparison between the pressure distribution on two-dimensional rods in rough boundary layers and in channel flows has never been attempted.

3. Results

3.1. *Parameterization of rough walls*

In the present paper, results for the three-dimensional geometries together with those for two surfaces with two-dimensional square bars with $w/k = 1$, one aligned with the flow (L_{SB}) and the other transverse to the flow (T_{SB}) are discussed. The three-dimensional roughness geometries are aligned square cubes (A_C), staggered square cubes (S_C), staggered cylinders (CI), staggered transversal wedges (TT), staggered longitudinal wedges (TL), and a combination of the last four ($E4$). The simulations, except for T_{SB} and for the smooth wall (C), were performed in a domain with dimension $L_1 = 8h$ and $L_3 = 4h$. Each element has a width equal to $0.2h$, thus there are 20 elements in the streamwise direction x_1, and 10 in the spanwise x_3 (x_i are dimensionless coordinates). The number of grid points in x_1 and x_3 are 400 and 200, respectively, so each element is discretized by 10 points. In the wall normal direction (x_2), a non-uniform grid with 161 points was used; 31 of the 161 points were located between the plane of the crests ($x_2 = -1$) and the bottom wall at $x_2 = -1.2$. To give an idea of the distribution and of the resolution of the elements, Figure 1(a) shows

	C	L_{SB}	T_{SB}	A_C	S_C	CI	TL	TT	$E4$
$u_{\tau S} \times 10$	0.42	0.42	0.43	0.44	0.46	0.45	0.43	0.46	0.43
$u_{\tau R} \times 10$	0.42	0.46	0.49	0.61	0.70	0.74	0.59	0.85	0.74
U_0^+	0.0	2.91	1.02	2.61	1.87	2.19	5.47	1.98	2.48
$u_2'^+/_w$	0.0	0.50	0.28	0.75	0.79	0.82	0.88	0.98	0.89
k^+	not	39.1	41.54	51.3	58.5	62.5	49.3	71.5	62.1
Δx^+	3.6	3.91	4.15	5.13	5.85	6.25	4.93	7.15	6.21
ΔU^+	0.0	5.56	4.52	10.1	10.6	11.7	12.0	13.1	12.0
$K_S \times 10$	not	0.45	0.50	2.35	4.20	4.57	2.24	6.27	3.94
$\delta \times 10$	not	−0.13	−0.18	−0.026	0.34	−0.68	0.52	−1.7	−1.08

TABLE 1. Quantities of interest from the simulations.

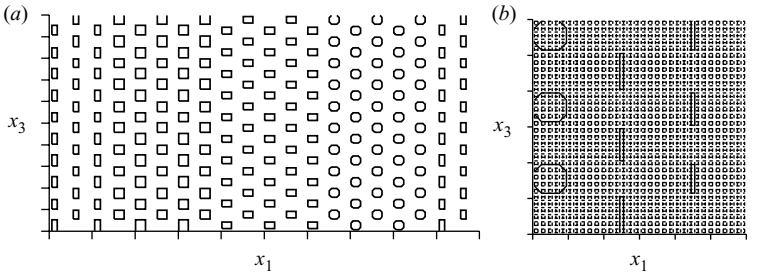

FIGURE 1. Three-dimensional roughness surfaces for the case $E4$ with elements with different shapes in: (a) plane (x_1, x_3) at $x_2 = -1.14$, and (b) by an enlargement at $x_2 = -1.06$.

the (x_1, x_3) planar view of the roughness with elements of different shape ($E4$). This (x_1, x_3)-plane cuts the elements at a height from the bottom equal to $0.06h$. The comparison of this horizontal plane with that at $0.14h$ (figure 1b) gives an idea of the shape and orientation of the wedge elements. In the enlargement (figure 1b), the grid is superimposed to estimate the resolution around the elements. To describe the cylindrical elements accurately, a greater resolution is required; however, the insufficient resolution creates a geometry different from that of the square cubes and of the wedges with sharp angles.

The Reynolds number is $Re = U_P h/\nu = 4200$, U_P is the reference velocity, because the simulations started from a laminar flow. The bulk velocity $U_b = 2/3U_P$, remains constant when the flow becomes fully turbulent. For all roughness configurations, the grid resolution near to the crest plane is $\Delta x_2^+ < 1$. At the centre of the channel, $\Delta x_2^+ \approx 6$, close to that for the other two directions. The differences among the several configurations considered can be appreciated by comparing the quantities in table 1; $u_{\tau R}$ is the dimensionless friction velocity of the rough surface, and $u_{\tau S}$ that of the smooth wall. The roughness Reynolds number $k^+ = k u_{\tau R} Re$ determines whether the flow is in the fully rough regime; from these values and from the arguments of Bandyopadyhay (1987), for two-dimensional bars, it follows that the present flows are fully rough. K_S and δ in (1.1) were obtained by a best fit of the values of U^+ around $U^+ = 8.48$. Although $\tilde{u}_2'|_w^+$ and K_S are not well correlated by increasing $\tilde{u}_2'|_w^+$, K_S increases. If the profiles in figure 2(a) are plotted versus $\hat{y} = (y + \delta)/K_S$ (the non-dimensional distance introduced by Nikuradse 1933 and used by Schlichting 1936), figure 2(b) is obtained. The values of U^+ from $y = \delta$ up to the location of maximum velocity are plotted in this figure, showing that the profiles overlap the

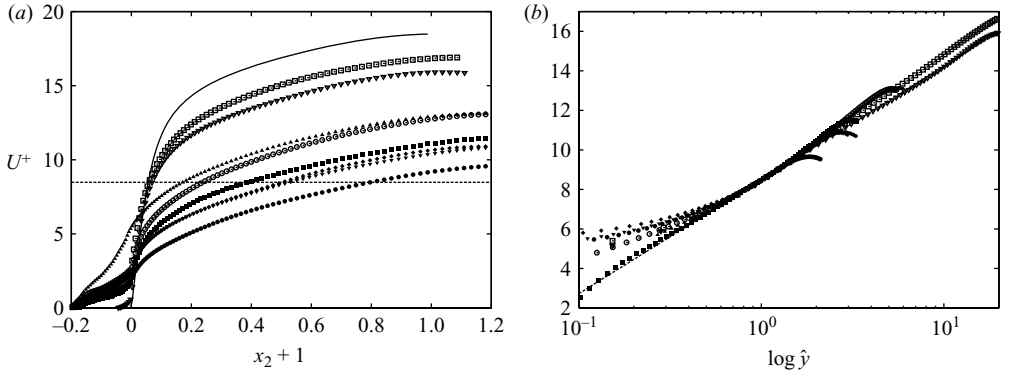

FIGURE 2. Streamwise velocity profiles in wall units versus: (*a*) the distance $y = x_2 + 1$ from the plane of the crests, the dashed line is $U^+ = 8.48$, (*b*) the dimensional distance $\hat{y} = (y + \delta)/K_S$, the dashed line is $U^+ = 5.75 \log(\hat{y}) + 8.48$; ——— , *C*, □, L_{SB}; ○, A_C, ■, S_C; ●, *TT*, ▲, *TL*, ▼, *CI*, △, T_{SB}, ◆, *E*4.

line $5.75 \log \hat{y} + 8.48$ for a different extension. In figure 2(*b*) y is the distance from the crest plane ($x_2 = -1$). Taking the origin of y at the bottom wall ($x_2 = -1.2$), as was done by Schlichting (1936), the values of K_S and δ would be different. This is a further indication that the quantities introduced by Nikuradse (1933) (K_S and δ) do not have an exact physical meaning, but have the property of producing a universal velocity law. By writing (1.1) also with the lengths in wall units, it becomes

$$U^+ = 5.55 + \kappa^{-1} \ln(y + \delta)^+ - \kappa^{-1} \ln K_S^+ - 2.94, \tag{3.1}$$

then $\Delta U_K^+ = \kappa^{-1} \ln K_S^+ - 2.94$ coincides with ΔU_C^+ in (1.2). A good correlation between ΔU_K^+ and $\tilde{u}_2'|_w^+$ is found, but not as good as that between ΔU^+, in (1.4), and $\tilde{u}_2'|_w^+$, described in the next paragraph.

To find a parameterization for the roughness function, it is convenient to start from (1.4), the well-accepted log-law for wall turbulent flows. Here, the virtual origin, which has a certain degree of arbitrariness, and which depends on the kind of surface, has been eliminated. Equation (1.4) holds for smooth walls, where, at $y = 0$, $U = 0$, in analogy with flow past rough walls at $\tilde{y} = 0$, should be $\tilde{U} = 0$. For the geometries considered here, the maximum height of the elements is constant, then $\tilde{y} = 0$ at the plane of the crests is the simplest assumption. At this location, an averaged streamwise velocity U_0 does exist, and $\tilde{U} = U - U_0 = 0$ at $\tilde{y} = 0$. In numerical simulation, the evaluation of U_0 is easy, on the other hand, in experiments, difficulties arise in measuring between the roughness elements. A satisfactory value of U_0 can be estimated by an extrapolation of a large set of measurements in a thin region near the plane of the crests. For the present simulations, $\tilde{U}^+$ versus $\tilde{y}^+$ is shown in figure 3(*a*); the straight line is given by (1.4) with $k = 0.41$, $B = 5.5$ and $\Delta U^+ = 0$. The large symbols indicate the points where ΔU^+ is calculated as the difference between the values at these points and the corresponding values on the dashed line (values in table 1). At low Reynolds number, the width of the log-law could be rather short; however, figure 3(*a*) shows that in the present DNS the log-law is long for a satisfactory evaluation of ΔU^+, in fact for the rough wall, R_τ is larger than that for the opposite smooth wall. Figure 3(*a*) shows that if the elements are aligned with the flow, the velocity profile presents a mild downward shift. The roughness function

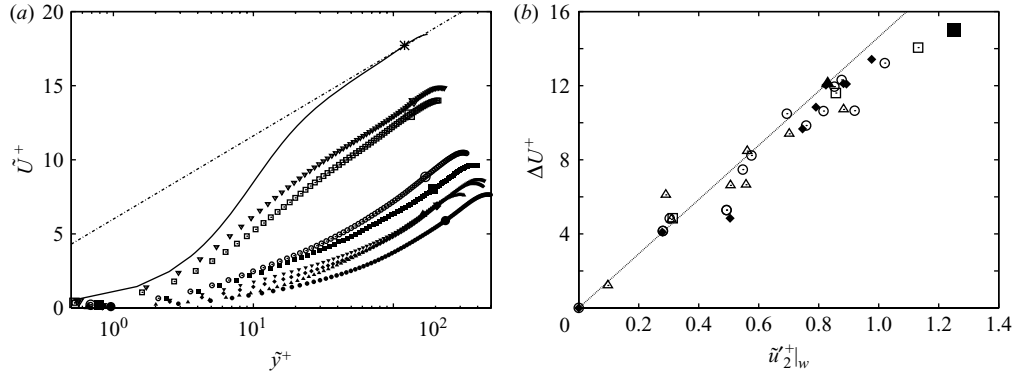

FIGURE 3. (*a*) Velocity profiles versus the distance from the plane of the crests; (*b*) roughness function versus the u_2' r.m.s. at the plane of the crests; in (*a*) the legend in figure 2(*a*), in (*b*) □, Burattini *et al.* (2008); ◆, present; ○, Leonardi *et al.* (2003); △, Orlandi & Leonardi (2006); ▲, Flores & Jiménez (2006); ■, Cheng & Castro (2002).

ΔU^+ increases when the flow impinges on transverse rough elements; the highest shift is found for transverse wedge elements (*TT*), which produce a large $\tilde{u}_2'|_w$.

DNSs with different boundary conditions for the three velocity components at the wall, have shown that large variations of drag and turbulence production are linked to u_2' variations. This has been demonstrated by Orlandi *et al.* (2003), showing that the principal effects of a rough surface can be mimicked by distributions of u_2'. Whereas Orlandi *et al.* (2003) used the u_2' distribution generated by DNS of two-dimensional square bars (Leonardi *et al.* 2003), Flores & Jiménez (2006) reached similar conclusions with synthetic velocity distributions. From these observations, Orlandi *et al.* (2006) and Orlandi & Leonardi (2006) presented a very good correlation of ΔU^+ with $\tilde{u}_2'|_w$, and even better with $\tilde{u}_2'^+|_w$. The previous data are added to the present results, with three-dimensional elements, to the results at high *Re* by Burattini *et al.* (2008), and to one of the flows simulated by Flores & Jiménez (2006). Flores & Jiménez (2006) used *ad hoc* boundary conditions for u_2' on a smooth wall. Burattini *et al.* (2008) showed that at various *Re*, the DNS profiles agree well with those measured in an experimental apparatus with an equal surface roughness. The measurements were taken by cross-wires, and it was not possible to evaluate $\tilde{u}_2'^+|_w$, even by extrapolating the data near the plane of the crests, therefore it was not possible to obtain the experimental values to insert in figure 3(*b*). However, the good comparison between the profiles suggests that the values of ΔU^+ and $\tilde{u}_2'^+|_w$ should be close to those by DNS (open squares) in figure 3(*b*). For three-dimensional staggered cubes, Cheng & Castro (2002) measured mean velocity and Reynolds stress profiles with LDV, these data were used to evaluate the roughness function in (1.4) which correlates well with $\tilde{u}_2'^+|_w$ (figure 3*b*).

Figure 3(*b*) shows that numerical and experimental data fit well with the relationship $\Delta U^+ = B/\kappa \tilde{u}_2'^+|_w$. For values of $\tilde{u}_2'^+|_w$ up to 0.8, the data agree well with the linear relationship, some disagreement is encountered at high $\tilde{u}_2'^+|_w$. In addition, figure 3(*b*) establishes a limit on the value of the roughness function, which can be estimated as $\Delta U^+ \approx 15$. An exact value can be found by performing more simulations or experiments; however, figure 3(*a*) shows that, to obtain $\Delta U^+ = 15$ at $y^+ \approx 200$, U^+ should be equal to 2, and, for $y^+ > 200$, U^+ should grow parallel to the log-law for smooth walls. This profile implies a large U_0 and small velocity gradients in the outer

region, a behaviour unlikely to be encountered in practical applications. In addition, we think that, for surfaces of practical interest, it is difficult that the flow field between the elements produces $\tilde{u}_2'^+|_w > 1.5$. Without a correction at high $\tilde{u}_2'^+|_w$, (1.4) becomes

$$\tilde{U}^+ = \kappa^{-1} \ln(\tilde{y}^+) + B \left(1 - \frac{\tilde{u}_2'^+|_w}{\kappa}\right), \tag{3.2}$$

which can be useful in engineering applications. The question then is how (3.2) can be useful when $\tilde{u}_2'|_w$ may not be known. In our opinion, the expression can be used in several ways, but other ways are also possible. Measured mean velocity profiles may be fitted to (3.2), to find $\tilde{u}_2'|_w$ that best reproduces the results; this is similar to how Nikuradze's (1.2) is used to find K_S.

Often the measure of the friction velocity is difficult, therefore (3.2) could be used to find the friction velocity $u_{\tau R}$ measuring the mean velocity and the normal to the wall velocity r.m.s. at the crests plane. Equation (3.2) can be of greater help in simulations: in RANS (Reynolds averaged Navier–Stokes) the Reynolds stress equations are introduced, and often it is necessary to simulate the near-wall region (low-Reynolds-number turbulence closures). The transport equation for the normal stress requires boundary conditions at the plane of the crests. By assigning $\tilde{u}_2'|_w$, (3.2) shows that we are mimicking a particular rough surface. The improvement with respect to the K_S approach is because $\tilde{u}_2'|_w$ enters into the system of equations. On the same grounds, $\tilde{u}_2'|_w$ could be of help in engineering LES, to avoid the description of the real rough surfaces, which requires a large number of grid points, especially for three-dimensional surfaces. In these simulations, the resolved vertical fluctuations to assign at the plane of the crests should be evaluated through (3.2).

It has been investigated whether a similar correlation between ΔU^+ and $\tilde{u}_3'^+|_w$ exists; for three-dimensional surfaces, the correlation is not as good as for $\tilde{u}_2'^+|_w$.

This new parameterization suggests that profiles of statistics related to $\tilde{u}_2'$ account for the complex physics of the thin layer near the plane of the crests, which in the next section is studied by the flow structure modifications.

3.2. *Flow structures of rough walls*

In previous DNS and experiments, it has been observed that the roughness reduces the structure anisotropy. The tendency towards isotropy has been quantified in several ways, for instance by two-point correlations, or by anisotropic maps (Leonardi *et al.* 2004). More recently POD (proper orthogonal decomposition) was used by Sen, Bhaganagar & Juttijudata (2007) to characterize the structures in the region near the roughness surface. Having found that $\tilde{u}_2'^+|_w$ characterizes the rough flows it is worth presenting the profiles of $\tilde{u}_2'^+$; figure 4(*a*) shows that, in the near-wall region, $\tilde{u}_2'^+$ depends on the kind of roughness elements, and differs from that of a smooth wall, with a tendency to be almost constant with y^+ near the roughness. This observation is useful in a laboratory for evaluating $\tilde{u}_2'|_w$ from a set of measurements near the roughness. Experimental data could complement the present findings, in fact, in a laboratory it is easier to increase *Re*, to investigate whether (3.2) also holds in practical flows. In addition, it is easier to find whether a limited value of ΔU^+ exists and to obtain the data for the eventual correction at high $\tilde{u}_2'^+|_w$. Despite the flat behaviour of $\tilde{u}_2'$ near the roughness, the size of the cross-wires is usually greater than the layer where $\tilde{u}_2'$ is constant, as can be appreciated in Burattini *et al.* (2008). From the measurements of Cheng & Castro (2002), it seems that LDV is appropriate for measuring u_2' as close as possible to the roughness surface.

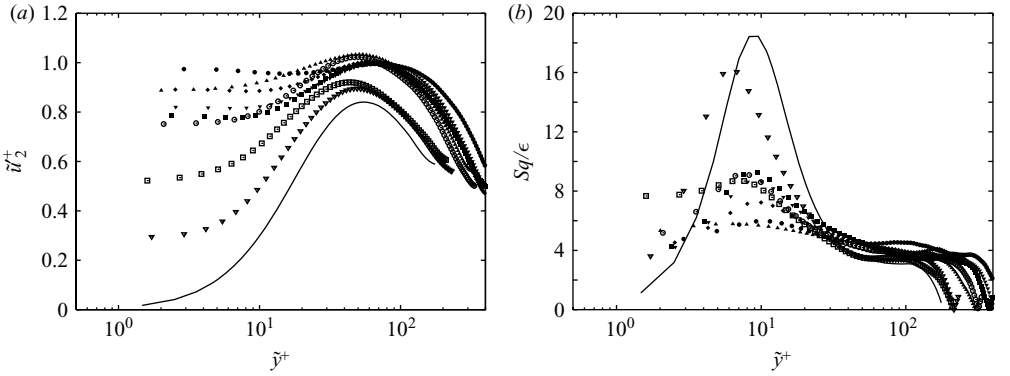

FIGURE 4. (*a*) Normal stress profiles and (*b*) the ratio between mean and turbulence time scales versus distance in wall units; legend as figure 2(*a*).

The ratio between the mean flow and the turbulence time scales, indicated by Sq/ϵ ($S = \mathrm{d}\langle u_1\rangle/\mathrm{d}y$, q is the turbulent kinetic energy and ϵ the rate of energy dissipation) is a further quantity characterizing the structure modification. Lee, Kim & Moin (1990) by DNS of channel and shear-layer flow disputed the old belief that the wall structures were related to the impermeability conditions, hence to the suppression of turbulence by the wall. Their homogeneous shear flow DNS demonstrated that elongated structures formed, and that the two-point correlations were similar to those in a plane channel, if an equal Sq/ϵ was found. When Sq/ϵ decreases, the structures become similar to those in isotropic turbulence. The profiles of Sq/ϵ in figure 4(*b*) show a reduction of the peak with respect to that of a smooth wall; the higher $\tilde{u}_2'|_w$ is, the smaller the peak. Their maxima remain within the buffer region, where, for a smooth wall, the streamwise vortices, those producing the turbulent kinetic energy, are located. Figure 4(*b*) shows that for T_{SB}, the values do not differ largely from those for C, hence small modifications of the low- and high-speed streaks should be expected, as was quantified by Leonardi *et al.* (2004). For the other geometries, the Sq/ϵ peak reduction is a consequence of a tendency to form structures similar to those in isotropic turbulence. These changes of the structures are later described by visualizations of a passive scalar.

Vorticity fluctuations account for the kind of flow structure, in particular, ω_2' represents the near-wall structures, and its contour plots are presented to show the low- and high-speed streaks. On a smooth wall $\tilde{\omega}_2' = \langle\omega_2'^2\rangle^{1/2} = 0$ at $y = 0$; it increases with y to reach a maximum in correspondence with the location of maximum turbulent energy production. Also, ω_1' is linked to the near-wall structures, with a relative minimum of $\tilde{\omega}_1'$ at $y^+ \approx 5$, the location of the centre of the near-wall vortices with a mean radius of about 10 wall units. Instead of plotting the profiles of $\tilde{\omega}_i'$, it is more appropriate to plot $d_{ij} = \langle\omega_i'\omega_j'\rangle/\tilde{\omega}_l'^2$, where $\tilde{\omega}_l'^2$ is the enstrophy. For isotropic turbulence $d_{ii} = 1/3$ (no summation), instead for smooth walls d_{22} tends to zero approaching the wall, and $d_{33} = 1 - d_{11}$ is the greatest. Figure 5(*a*) shows that, in the presence of rough walls, the relative minimum of d_{11}, at $y^+ \approx 5$, increases. For, TT, strong disturbances are produced near the roughness surface, and the profile of d_{22} becomes fairly constant; the same value, approximately equal to 1/3, for d_{11} indicates a flow isotropy in the whole channel.

To understand better the effects of the roughness near the plane of the crests, the joint probability density functions (j.p.d.f.) between $\sigma_{u2} = u_2'/\tilde{u}_2'$ and $\sigma_{o2} = \omega_2'/\tilde{\omega}_2'$ have

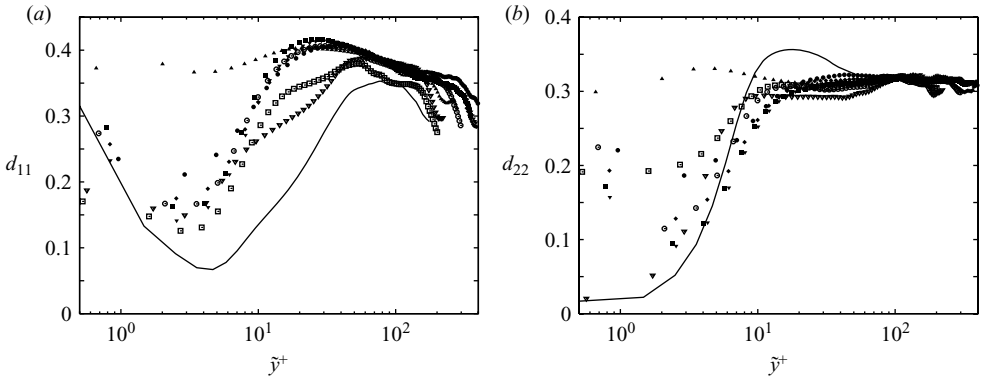

FIGURE 5. Vorticity correlations coefficients (*a*) d_{11}, (*b*) d_{22} versus the distance in wall units; legend as in figure 2(*a*).

been calculated. The joint p.d.f. accounts for the intermittency of the events and for the correlation between the two quantities. The intermittency reduces if the contours are more clustered near the origin. Figure 6(*a*), for the smooth wall, shows elongated tails for σ_{u2}, and this agrees with the Kim, Moin & Moser (1987) observation that the flatness factor for u_2' ($F_{u2} = \langle u_2'^4 \rangle / \langle u_2' \rangle^2$) is greater than that of the other two velocity components. The long tails are related to the bursting events, which for a smooth channel, are intense, and rare. We recall that the p.d.f. of the quantities in the abscissa and ordinate of figure 6 can be obtained by a summation in the other direction. For transverse (T_{SB}, figure 6*b*) and longitudinal (L_{SB}, figure 6*c*) square bars the probability of having a very strongly events decreases, but not as strongly as for the three-dimensional elements. The T_{SB} with $w/k = 1$ generates weak recirculating flows, and the ejections from the cavity do not largely modify the p.d.f. of σ_{u2} with respect to that for a smooth wall. To corroborate the weakness of the recirculating flow inside the square cavities of T_{SB}, the Reynolds number $R_K = U_0 k/\nu$, from the values in table 1, is $R_K = 42$, proving the formation of a weak recirculation. For L_{SB}, the secondary motion, within the square bars, is stronger and the p.d.f. of σ_{u2} has shorter tails. The different strengths of the flows inside the L_{SB} and T_{SB} surfaces were described by Orlandi & Leonardi (2006) and are not repeated here. The values of F_{u2} are given in the caption to figure 6, showing that for three-dimensional surfaces a Gaussian distribution, typical of isotropic turbulence is obtained. In the evaluation of the joint p.d.f., the events with $\sigma > 6$ were neglected, then the values of the flatness factors are slightly smaller than those evaluated by accounting for all the events. For instance, for the smooth channel, at $y^+ = 4.9$, with the threshold (events with $\sigma \leqslant 6$) $F_{u1} = 2.70$, $F_{u2} = 5.90$ and $F_{u3} = 2.78$ were found, while accounting for all the events $F_{u1} = 2.70$, $F_{u2} = 7.90$ and $F_{u3} = 3.93$, which agree with those in figure 18(*b*) of Kim *et al.* (1987).

A negative correlation coefficient $\sigma_{u2o2} = \langle u_2' \omega_2' \rangle / (\tilde{u}_2' \tilde{\omega}_2)$ is related to the larger contribution of the fourth quadrants with respect to the others. For T_{SB}, the cancellation between positive and negative quadrants gives a small σ_{u2o2}. Although figure 6 shows that the correlation coefficients do not largely vary, the roughness effects are clearer on $\langle u_2' \omega_2' \rangle$. For a flat channel, Rogers & Moin (1987) found that the total helicity ($\langle u_i' \omega_i' \rangle$) remains small across the whole channel. To investigate the effects of the roughness on the total helicity, the three helicity components in the smooth channel are compared with those for the *TT* roughness, the elements

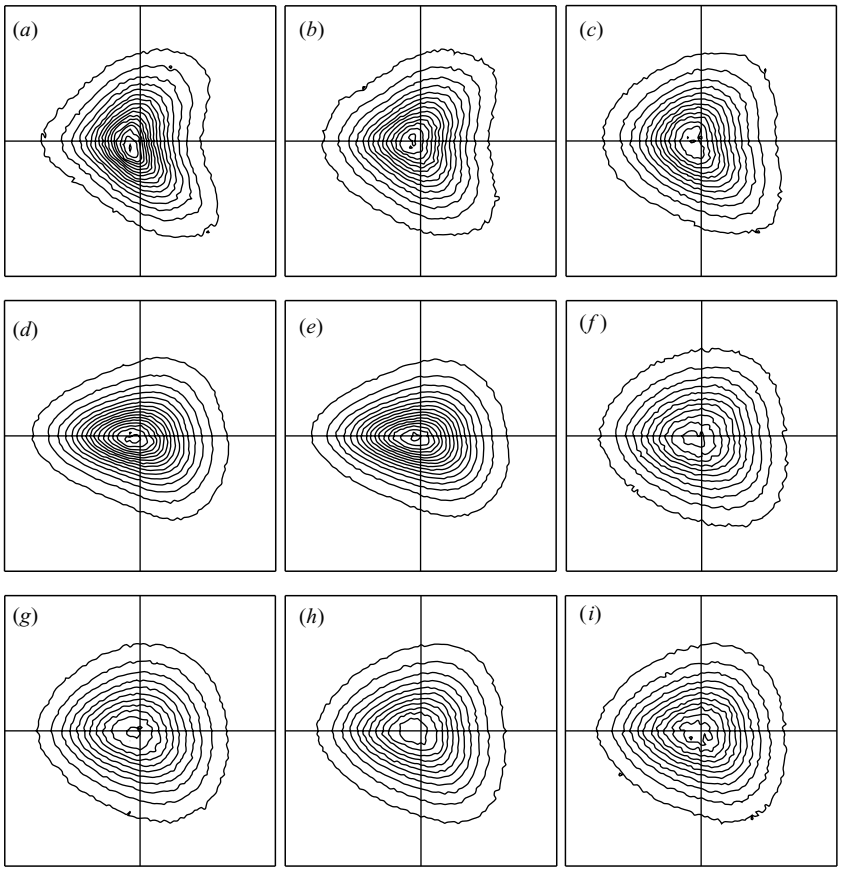

FIGURE 6. Joint p.d.f. of σ_{u2} (abscissa) and σ_{o2} (ordinate), contours with increment $\Delta = 0.004$, with the box extending from -3 to 3 evaluated at $y = 0.07$; (*a*) *C*, $F_{u2} = 5.42$, (*b*) T_{SB}, $F_{u2} = 4.24$, (*c*) L_{SB}, $F_{u2} = 3.86$, (*d*) A_C, $F_{u2} = 3.34$, (*e*) S_C, $F_{u2} = 3.34$, (*f*) *TL*, $F_{u2} = 3.16$, (*g*) *TT*, $F_{u2} = 3.19$, (*h*) *CI*, $F_{u2} = 3.31$, (*i*) *E*4, $F_{u2} = 3.24$.

producing the strongest ejections. Figure 7(*a*) shows that for smooth walls, the three components are small, and that for *TT*, two of the components are large, and that $\langle u_1'\omega_1' \rangle$ remains small. Having demonstrated that $\langle u_2'\omega_2' \rangle$ is the largest component, and that the imbalance with $\langle u_3'\omega_3' \rangle$ creates a total helicity density in the presence of roughness, it is worth seeing how the profiles of $\langle u_2'\omega_2' \rangle$ change near the plane of the crests. Figure 7(*b*) shows that this helicity component is, large for three-dimensional staggered elements; where the flow, impinging on the front face of the elements, produces large $\partial u_1/\partial x_1$, and for incompressibility, large $\partial u_2/\partial x_2$. These events do not occur for the T_{SB} surface, with weak recirculating regions, and for L_{SB} and A_C where the flow remains parallel to the elements.

3.3. *Flow visualizations*

A passive scalar can be used to obtain a qualitative picture of the changes in the structures; for instance, in a laboratory, flow visualizations are made by injecting smoke or dye inside the rough elements, and from the photographs, the vorticity field can be drawn. In the numerical simulations, the vorticity field is accessible and contour plots in horizontal planes emphasize the differences among the three ω_i' components. In DNS, sophisticated vortex-detection methods together with flow animations are

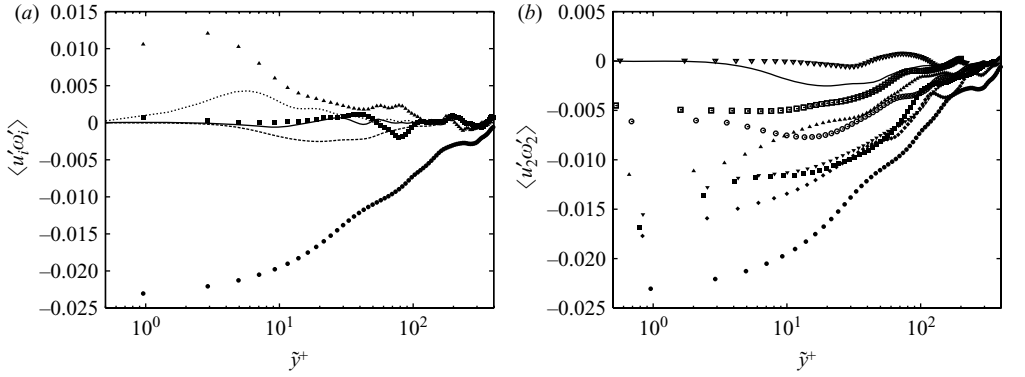

FIGURE 7. Profiles of (a) the three helicity density components for: smooth wall (lines), TT surface (symbols), (——— , ■, $i=1$; . . . , ●, $i=2$; ····· , ▲, $i=3$); (b) $\langle u_2'\omega_2'\rangle$ (legend as figure 2a), the vertical distance $\tilde{y}$ is taken from the plane of the crests and is normalized in wall units.

often used to study the near-wall complex physics. In this paper, to give insights to the experimentalists on what they should expect, visualizations, similar to those in laboratories, are performed. Then, the equation for the passive scalar θ was solved

$$\frac{\partial\theta}{\partial t}+\frac{\partial\theta u_j}{\partial x_j}=\frac{1}{Re\,Pr}\frac{\partial^2\theta}{\partial x_j^2}. \tag{3.3}$$

The use of the Prandtl number (Pr) implies that θ represents the temperature field created by keeping the rough wall at a constant dimensionless temperature $\theta_R=1$. The opposite smooth wall has a constant temperature $\theta_S=-1$. $Pr=1$ is a value not too different from the Prandtl numbers typical of water, or air. On the other hand, to reproduce dye in water, Pr should be substituted by the Schmidt number (Sc) of $O(10^3)$. In these circumstances the simulations require large computer resources. From the numerical side, the immersed boundary technique treats the passive scalar as the velocity field, with only a small increase in memory occupancy and computational time.

To investigate more clearly the influence of the type of roughness surface on θ', the plots in figure 8 were evaluated at $x_2=-0.96$, a distance closer to the surface than $x_2=-0.93$ where the joint p.d.f.s in figure 6 were calculated. The values of the correlation between θ' and the three velocity components are given in table 2. The strong negative correlation between θ' and u_1' explains why, in the photographs taken in a laboratory, the low-speed streaks are bright and the high-speed streaks are dark. The markers, in fact, reside for a longer time in the low-speed streaks. The correlation between θ' and u_3' is small, and the turbulent heat flux $\langle\theta' u_2'\rangle$, as well as $\tilde{\theta}'$ increases when $\tilde{u}_2'$ increases. Therefore, three-dimensional roughness surfaces produce an increment on the heat transfer with respect to that for a smooth wall or to that in the presence of surfaces with two-dimensional elements.

The contours for $\theta'/\tilde{\theta}'$ with $\tilde{\theta}'=\langle\theta^{2\prime}\rangle^{1/2}$ are shown in figure 8. It should be recalled that $\tilde{\theta}'$, at a distance from the plane of the crests, depends on the kind of surface. Figure 8(a) shows clearly the low- and high-speed streaks typical of smooth channels. For transverse square bars (T_{SB}, figure 8b) the streaks become shorter. Even if the disturbances are weaker than that relative to other rough surfaces, they reduce the length and the coherence of the near-wall structures. The proof that small disturbances affect the structures comes from a comparison between figure 8(c), for L_{SB}, and

	C	L_{SB}	T_{SB}	A_C	S_C	CI	TL	TT	$E4$
$\tilde{u}'_2 \times 10^2$	0.817	2.840	2.170	4.900	5.560	6.190	5.380	8.130	6.570
$\tilde{\theta}' \times 10^2$	0.294	0.639	0.605	1.080	1.360	1.400	0.970	1.830	1.500
$-\langle\theta' u'_1\rangle \times 10^2$	0.882	0.924	1.380	1.120	1.110	1.070	0.848	0.853	1.010
$\langle\theta' u'_2\rangle \times 10^3$	0.380	1.360	1.320	2.770	3.250	3.600	2.700	3.970	3.440
$\langle\theta' u'_3\rangle \times 10^4$	0.199	0.150	1.840	−1.950	−1.900	0.065	0.324	−2.040	1.420
F_{u2}	7.890	4.945	5.621	3.894	3.954	3.707	3.294	3.220	3.519
F_θ	2.821	2.855	2.553	2.880	3.061	2.977	3.209	3.454	3.331

TABLE 2. Statistics related to θ at $x_2 = -0.96$.

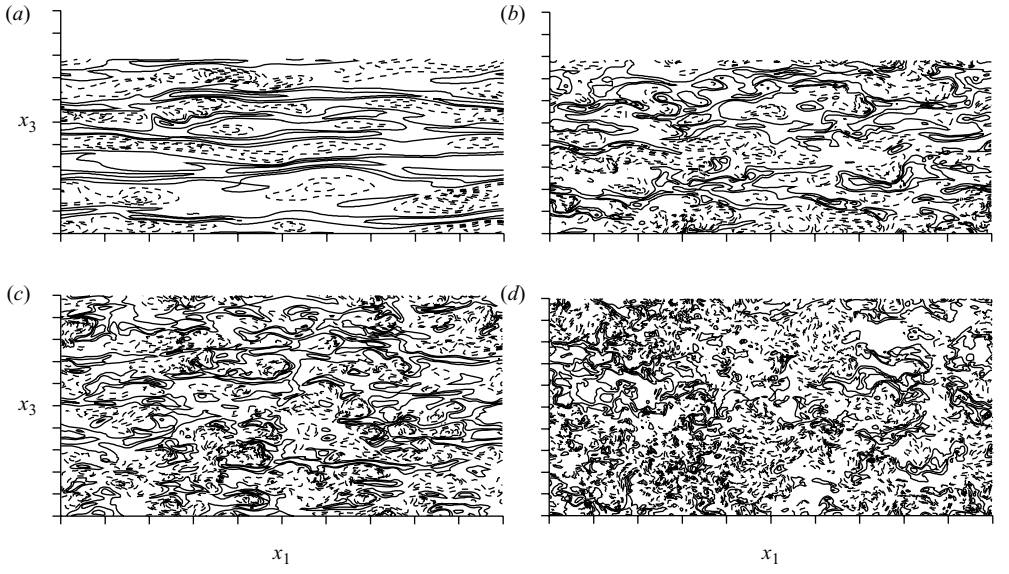

FIGURE 8. Contour plots of $\theta'/\tilde{\theta}'$ with increments $\Delta = 0.6$ solid positive, dashed negative: (*a*) C, (*b*) T_{SB} ($L_3 = 2\pi h$), (*c*) L_{SB}, (*d*) $E4$ ($L_3 = 8h$).

figure 8(*b*) for T_{SB}; in figure 8(*c*), the streaks are barely detectable although table 2 gives similar values of $\tilde{u}'_2$. The reduction of longitudinal coherence increases in the other configurations, the small differences with the TT surface suggest presenting the contours for this geometry (figure 8*d*), where high positive peaks are correlated with the strongest ejections. The common result in figure 8 is that the underlying roughness structure is not recognizable through flow visualizations.

To have a quantitative idea of the temperature fluctuations, the p.d.f. of $\sigma_t = \theta'/\tilde{\theta}'$ were evaluated at two planes, the first at $x_2 = -0.96$ (figure 9*a*) and the second at $x_2 = 0$. (figure 9*b*). In both planes, the negative skew property of the fluctuations is emphasized, which agrees with the laboratory observations that the bright regions, corresponding to the low-speed streaks, are more elongated and visible than the dark regions. The comparison between the two planes, far apart from each other, shows that the differences are greater for the smooth wall than for the surfaces generating strong ejections. This is a further indication that for three-dimensional rough surfaces the near-wall structures are more isotropic. In table 2, the values of the flatness factors for u'_2 and θ' accounting for all the events are given. The comparison between F_{u2} and F_θ supports the observation that in the thermal field, the imprinting of the different

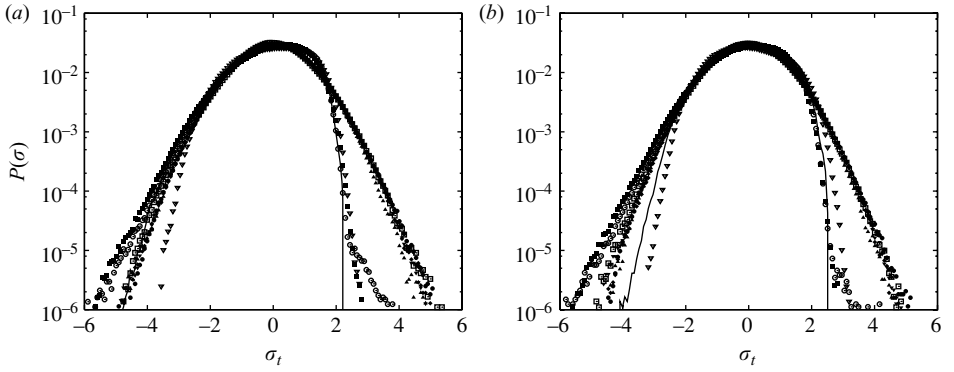

FIGURE 9. Probability density distribution for $\sigma_t = \theta'/\tilde{\theta}'$ at (*a*) $x_2 = -0.96$, (*b*) at the centre of the channel; legend as figure 2(*a*).

surfaces does not occur. Further studies are necessary for a deeper understanding of the heat transfer in the presence of rough surfaces, and in particular to separate the contribution of turbulent heat from that of thermal conduction.

4. Conclusions

DNS results of different kinds of three-dimensional rough surfaces have been performed, following the direction suggested by Schlichting (1936), who criticized the decision of Nikuradse (1933) to use sand grain, because of the difficulty of reproducibility. DNSs of surfaces with random disturbances require a large number of grid points to account for the spatial variations; a first attempt was by Yakhot, Grinberg & Nikitin (2005) using two-dimensional simulations of flows past randomly shaped stenoses. This can be considered a numerical exercise, because the flow physics in two dimensions is different from that in three dimensions. The present numerical method can be applied to random surfaces, but it requires access to a large number of parallel processors in supercomputer centres. The aim of the present study is to have a robust confirmation of the validity of the parameterization of the roughness function with $\tilde{u}'_2|_w$. A simple expression for the velocity profiles in the log region has been found, which can be useful in practical applications as well as in theoretical considerations. In our work we followed Nikuradse; at that time, the best way to understand the roughness flow physics was in a laboratory, and from accurate measurements, he derived the relationship in (1.1) using two length scales. This expression was often used in modelling rough flows as reported by Belcher *et al.* (2003), for example, Good & Belcher (1999) described how to use the relationship in practical problems. The present DNS allows us to derive (3.2) where, instead of two *ad hoc* length scales, two well-defined physical quantities appear. We think that this should be considered an improvement towards a roughness function parameterization. The usefulness of the correlation in LES or RANS modelling was discussed in the paper, and in addition we suggested how (3.2) could be used in the laboratory to evaluate $u_{\tau R}$ from measured values of the mean velocity and of the normal r.m.s. velocities at the crest heights.

The three components of the helicity density, which were never considered in the context of rough flows, have been evaluated. It has been found that one component $\langle u'_1\omega'_1\rangle$ is negligible and that $\langle u'_2\omega'_2\rangle$ prevails on $\langle u'_3\omega'_3\rangle$. Therefore, the helicity density can be considered to be a further quantity characterizing the kind of roughness. The

helicity density was also used to characterize flows with external forces. For instance, by rotating a pipe along the flow direction, helical structures form (Orlandi 1997), leading to drag reduction and to helicity density increase. The drag reduction was related to the formation of more ordered helical structures, which oscillate less than the structures near smooth walls. In rough flows, the strong ejections (u'_2), from the rough elements, promote large fluctuation of u'_3, with an increase in disorder and a tendency toward isotropy. Whereas in isotropic turbulence the velocity fluctuations have a random orientation, in rough flows the surface produces a predominant direction along which the vorticity is aligned. The tendency towards isotropy has been characterized by profiles of d_{22}. Visualizations of a passive scalar lead to the same conclusions, and in addition give insights into the complex physics of heat transfer near rough walls. This topic requires further studies which are currently being undertaken.

As a final comment to the large number of experimental, theoretical and numerical studies available in the literature, we think that it is time to try to overcome and perhaps to eliminate the characterizations of rough flows used until now. For instance, the sharp transition between k and d type is not physical, the transition should be smooth as shown in Leonardi *et al.* (2007). The parameterization with $\tilde{u}'_2|_w$ allows the classification of any kind of geometry, by eliminating the shape of the elements. This could be important in LES of real flows, where it is not feasible to use grids describing the details of the rough surface. A profitable way should rely on low-Re DNS for a large number of surfaces, to create a table, where at each surface there is a corresponding value of $\tilde{u}'_2|_w$ and U_0. This step is analogous to the Nikuradse (1933) charts, relating the velocity profiles to the equivalent sand grain thickness. The roughness shape could be replaced by synthetic boundary conditions, on a flat wall, given by a constant U_0 and a random distribution of u'_2 with the desired $\tilde{u}'_2|_w$. A subgrid model should be more effective for rough than for smooth walls, from the observation of an increase of isotropy near the plane of the crests.

The support of a MIUR 60 % grant is acknowledged, and that of a PRIN to purchase a cluster of PCs. CASPUR is acknowledged for computer resources. The first draft was written during a pleasant summer in the Villa Monti in Toscana.

REFERENCES

del Álamo, J. C., Jiménez, J., Zandonade, P. & Moser, R. D. 2004 Scaling of the energy spectra of turbulent channels. *J. Fluid Mech.* **500**, 135–144.

Bandyopadhyay, P. R. 1987 Rough-wall turbulent boundary layers in the transition regime. *J. Fluid Mech.* **180**, 231–266.

Belcher, S. E., Jerram, N. & Hunt, J. C. R. 2003 Adjustment of a turbulent boundary layer to a canopy of roughness elements. *J. Fluid Mech.* **488**, 369–398.

Bhaganagar, K., Kim, J. & Coleman, G. 2004 Effect of roughness on wall-bounded turbulence. *Flow Turbulence Combust.* **72**, 463–492.

Burattini, P., Leonardi, S., Orlandi, P. & Antonia, R. A. 2008 Comparison between experiments and direct numerical simulations in a channel flow with roughness on one wall. *J. Fluid Mech.* **600**, 403–426.

Cheng, H. & Castro, I. P. 2002 Near wall flow over urban-like roughness. *Boundary-Layer Met.* **104**, 229–259.

Clauser, F. H. 1954 Turbulent boundary layers in adverse pressure gradients. *J. Aero. Sci.* **21**, 91–109.

Coceal, O., Thomas, T. G., Castro, I. P. & Belcher, S. E. 2006 Mean flow and turbulence statistics over groups of urban-like cubical obstacles. *Boundary-Layer Met.* **121**, 491–519.

Fadlun, E. A., Verzicco, R., Orlandi, P. & Mohd-Yusof, J. 2000 Combined immersed boundary finite-difference methods for three-dimensional complex flow simulations. *J. Comput. Phys.* **161**, 35–60.

Flores, O. & Jiménez, J. 2006 Effect of wall-boundary disturbances on turbulent channel flows. *J. Fluid Mech.* **566**, 357–376.

Furuya, Y., Miyata, M. & Fujita, H. 1976 Turbulent boundary layer and flow resistance on plates roughened by wires. *Trans. ASME* I: *J. Fluids Engng* **98**, 635–644.

Good, K. & Belcher, S. E. 1999 On the parameterisation of the effective roughness length for momentum transfer over heterogeneous terrain. *Boundary-Layer Met.* **93**, 133–154.

Hama, F. R. 1954 Boundary layer characteristics for smooth and rough surfaces. *Trans. Soc. Nav. Archit. Mar. Engrs* **62**, 333–358.

Jiménez, J. 2004 Turbulent flows over rough walls. *Ann. Rev. Fluid Mech.* **36**, 173–196.

Kim, J., Moin, P. & Moser, R. 1987 Turbulence statistics in fully developed channel flow at low Reynolds number. *J. Fluid Mech.* **177**, 133–166.

Lee, M. J., Kim, J. & Moin, P. 1990 Structure of turbulence at high shear rate. *J. Fluid Mech.* **216**, 561–583.

Leonardi, S. & Orlandi, P. 2004 A numerical method for turbulent flows over complex geometries. *ERCOFTAC Bull.* **62**, 41–46.

Leonardi, S., Orlandi, P., Smalley, R. J., Djenidi, L. & Antonia, R. A. 2003 Direct numerical simulations of turbulent channel flow with transverse square bars on the wall. *J. Fluid Mech.* **491**, 229–238.

Leonardi, S., Orlandi, P., Djenidi, L. & Antonia, R. A. 2004 Structure of turbulent channel flow with square bars on one wall. *Intl J. Heat Fluid Flow* **25,** 384–392.

Leonardi, S., Orlandi, P. & Antonia, R. A. 2005 A method for determining the frictional velocity in a turbulent channel flow with roughness on the bottom wall. *Exps. Fluids* **38**, 796–800.

Leonardi, S., Tessicini, F., Orlandi, P. & Antonia, R. A. 2006 DNS and LES of turbulent flows over rough surfaces. *AIAA J.* **44**, 2482–2487.

Leonardi, S., Orlandi, p. & Antonia, R. A. 2007 Properties of d and k type roughness in a turbulent channel flow. *Phys. Fluids.* **19**, Dec.

Nikuradse, J. 1933 Stromungsgesetze in rauhen rohren. Forsch. Ing.-Wes. No. 361. Also Laws of flow in rough pipes. *NACA TM* 1292 (1950).

Orlandi, P. 1989 Numerical solution of 3-D flows periodic in one direction and with complex geometries in 2-D. *Annu. Res. Briefs, Center for Turbulence Res.* pp. 215–230.

Orlandi, P. 1997 Helicity fluctuations in rotating and non-rotating pipes. *Phys. Fluids* A **9**, 2045–2056.

Orlandi, P. 2000 *Fluid Flow Phenomena: A Numerical Toolkit*. Kluwer.

Orlandi, P. & Leonardi, S. 2006 DNS of turbulent channel flows with two and three-dimensional roughness. *J. Turbulence* **7**, no. 53.

Orlandi, P., Leonardi, S., Tuzi, R. & Antonia, R. A. 2003 DNS of turbulent channel flow with wall velocity disturbances. *Phys. Fluids* **15**, 3497–3600.

Orlandi, P., Leonardi, S. & Antonia, R. A. 2006 Turbulent channel flow with either transverse or longitudinal roughness elements on one wall. *J. Fluid Mech.* **561**, 279–305.

Perry, A. E., Schofield, W. H. & Joubert, P. N. 1969 Rough wall turbulent boundary layers. *J. Fluid Mech.* **37**, 383–413.

Raupach, M. R., Antonia, R. A. & Rajagopalan, S. 1991 Rough-wall turbulent boundary layers. *Appl. Mech. Rev.* **44**, 1–25.

Rogers, M. M. & Moin, P. 1987 Helicity fluctuation in incompressible turbulent flows. *Phys. Fluids* **30**, 2662–2671.

Schlichting, H. 1936 Experimental investigation of surface roughness. *NACA TM* 823.

Sen, M., Bhaganagar, K. & Juttijudata, V. 2007 Application of proper orthogonal decomposition (POD) to investigate turbulent boundary layer in a channel with rough-walls. *J. Turbulence* **8**, no. 41.

Yakhot, A., Grinberg, L. & Nikitin, N. 2005 Modeling rough stenoses by an immersed-boundary method. *J. Biomech.* **38**, 1115–1127.

Waigh, D. R. & Kind, R. J. 1998 Improved aerodynamic charaterization of regular three-dimensional roughness. *AIAA J.* **36**, 1117–1119.